In press, Journal of the American Ceramic Society LBNL-46789

High-Temperature Morphological Evolution of Lithographically Introduced Cavities in Silicon Carbide

Takayuki Narushima[†,✣] and Andreas M. Glaeser[✣]

Department of Materials Science and Mineral Engineering,
University of California
&
Center for Advanced Materials
Lawrence Berkeley National Laboratory, Berkeley, CA 94720

Abstract

Internal cavities of controlled geometry and crystallography were introduced in 6H silicon carbide single crystals by combining lithographic methods, ion beam etching, and solid-state diffusion bonding. The morphological evolution of these internal cavities (negative crystals) in response to anneals of up to 128 h duration at 1900°C was examined using optical microscopy. Surface energy anisotropy and facetting have a strong influence on both the geometric and kinetic characteristics of evolution. Decomposition of $\{1\bar{2}10\}$ cavity edges into $\{10\bar{1}x\}$ facets was observed after 16 h anneals, indicating that $\{1\bar{2}10\}$ faces are not components of the Wulff shape. The shape evolution kinetics of penny-shaped cavities were also investigated. Experimentally observed evolution rates decreased much more rapidly with those predicted by a model in which surface diffusion is assumed to be rate-limiting. This suggests that the development of facets, and the associated loss of ledges and terraces during the initial stages of evolution results in an evolution process limited by the nucleation rate of attachment/detachment sites (ledges) on the facets.

[†] Now at Department of Metallurgy, Tohoku University, Sendai 980-8579, Japan
[✣] Member, American Ceramic Society

Disclaimer

Copyright

Introduction

Studies of the morphological evolution of isolated crystals and cavities, of particles within powder compacts and of cracklike defects can contribute to our understanding of microstructural and property evolution during processing as well as during subsequent use at elevated temperatures. Such studies in conjunction with theoretical modelling can be useful in identifying the dominant mass transport mechanism, can help quantify the driving force for mass transfer, and can define the time-temperature conditions required for desired degrees of microstructural change. As pointed out by Gupta [1, 2], strong parallels exist between the microstructural changes that occur during high-temperature crack healing and those that arise in sintering. Thus, the findings of model studies of one process can impact our understanding of a broader range of phenomena.

Fundamental studies of crystal or pore shape changes in crystalline solids provide a means of assessing the mechanism of mass transport, and if equilibrium shapes are attained, can also be used to determine the relative energy of the surfaces that define the equilibrium or Wulff shape. For ceramics, internal cavities (negative crystals) offer several important advantages over isolated particles as the basis for such studies. These cavities are isolated from the external environment, thus reducing the potential for substantial mass loss due to vaporization and of inadvertent contamination. In addition, if the ceramics are transparent, the shape changes can be monitored nondestructively using optical microscopy, and examined with greater spatial resolution after anneals are completed.

An experimental method based on the sequential application of photolithography, ion beam etching, and solid-state diffusion bonding has been developed to produce intragranular cavities (negative crystals) of controlled geometry and controlled crystallography in ceramics [3, 4]. Prior work has focussed on model studies of surface properties in doped and undoped sapphire. The effects of dopants and crystal orientation on crack healing [5-7] and on Rayleigh instabilities [6-9] as well as the effects of dopants and temperature on relative surface energies (the Wulff shape [10, 11]) have been reported in the literature.

Silicon carbide is a model covalent, non-oxide material that is attractive for high-temperature structural applications by virtue of its high physical and chemical stability [12]. The size, shape, spatial

distribution and morphological evolution of flaws in silicon ceramics will impact the resulting mechanical behavior. Silicon carbide is also a wide band gap semiconductor, with potential for use at elevated temperatures [13-16]. Reports of the influence of surface energy anisotropy and anisotropy of surface diffusion on crystal growth have appeared in the literature [17, 18]. Therefore, efforts were made to adapt the methods previously used to examine sapphire surfaces and to apply them to silicon carbide. The present paper constitutes a first report of the use of such microdesigned internal defect structures to investigate the high-temperature properties of surfaces in single crystal silicon carbide.

Experimental Procedure

Sample Preparation

6H silicon carbide (α-type) single crystal wafers, 35 mm in diameter and 0.33 mm thick (Cree Research Inc., Durham, NC) with either silicon-terminated or carbon-terminated surfaces were employed in the present study. The surface orientation of the wafer is {0001} ± 0.5°. The wafers used were n-type (N doping) with a resistivity of 0.040 to 0.090 Ω·cm.[†]

All photolithographic processing was conducted in a class 100 clean room.[❖] After the silicon carbide single crystal was dried in air for 5 min at 120°C, a 1.5 μm thick layer of positive photoresist (Microposit s1818, Shipley, Inc., Marlborough, MA) was applied to the {0001} face by spin-coating at 5500 rpm. After a 20 min bake-out at 90°C, the photoresist was selectively exposed by UV radiation. The exposure pattern is dictated by the pattern of features in a mask; two different masks were used in the present work. The mask patterns have been described elsewhere [7, 19]. The exposed positive photoresist can be selectively removed with a developer (Microposit Developer Concentrate, Shipley Inc., Marlborough, MA). The patterned photoresist layer was hard-baked in air for 20 min at 120°C. The silicon carbide wafer was then etched using an argon ion beam. As discussed previously, this process etches the exposed silicon carbide surface, and the photoresist, transferring the mask pattern into the wafer. At an accelerating voltage of 1.1 kV and an argon pressure of 1.3×10^{-2} Pa, the etch rate was ≈0.9 μm/h. Etch

[†] In the ensuing discussion, the material is simply referred to as silicon carbide, however, we emphasize that the results are relevant to a doped material, and the conclusions drawn from these results may not apply to undoped or "pure" silicon carbide.
[❖] The concentration of airborne particles larger than 0.5 μm is less than $3.53 \times 10^3/m^3$ or $100/ft^3$.

depth was adjusted by adjusting the etching time, and conditions leading to etch depths of either 0.25 μm or 0.15 μm were employed. The silicon carbide single crystal was continuously rotated during ion milling to promote uniform etching and features of uniform etch depth. After etching, the residual photoresist was removed with acetone. Subsequently, the silicon carbide was cleaned by sequential immersion in $5H_2O$:H_2O_2:NH_4OH, $6H_2O$:H_2O_2:HCl and $10H_2O$:HF solutions, which remove organic residue, trace metal and oxide films, respectively.

Internal cavities (negative crystals) were produced by diffusion bonding etched and unetched silicon carbide single crystal pieces of common surface orientation, aligned to produce at worst a 1-2° twist boundary. The bonds were produced by mating an etched silicon-terminated and unetched carbon-terminated face or an etched carbon-terminated and unetched silicon-terminated face.✣ Bonding was performed in a graphite element vacuum hot press. Samples were heated at 5°C/min to 1400°C, held for 2 h with an applied load of 15 MPa, and then heated at 5°C/min to 1500°C where a load of 20 MPa was applied for an additional 2 h. Samples were cooled at 10°C/min. Well-bonded interfaces were obtained. Vacuum during the entire bonding process was $<2 \times 10^{-3}$ Pa.

Heat Treatment

All anneals were performed in a molybdenum-mesh resistance furnace under vacuum conditions ($<2 \times 10^{-3}$ Pa). Samples were annealed at 1900°C for times of up to 128 h (460.8 ks). Specimens were placed in a high-purity carbon crucible (Tokai Carbon Co. Ltd., Tokyo, Japan) which was baked-out at 1950°C under a vacuum of $<2 \times 10^{-3}$ Pa prior to usage. After each anneal, both outer surfaces of specimens were polished with progressively finer grit diamond, finishing with 1 μm paste. Since silicon carbide single crystals are transparent even after diffusion bonding, the shape changes of internal cavities could be monitored using optical microscopy with transmitted light. Since this inspection process is nondestructive, it was possible to anneal samples repeatedly at 1900°C, and track the morphological evolution of internal voids.

✣ Argon ion beam etching of 6H SiC crystals has been reported to produce changes in the surface structure and composition [20]. As a result, the cavities that result in these two cases, although indistinguishable if the opposing surfaces were both of a perfect crystal, might in this case evolve differently.

Results and Discussion

Facetting Behavior

Arrays of rectangular cavities, 200 μm × 100 μm × 0.25 μm in size, with the large faces lying parallel to the {0001} faces of silicon carbide, and long edges parallel to the $<1\bar{2}10>$ and $<10\bar{1}0>$ directions were produced. An example of a representative cavity etched into a silicon-terminated surface, after bonding but prior to any annealing is provided in Figure 1a. Figures 1(b–d) illustrate the morphology of a specific (representative) flaw after progressively longer anneals at 1900°C. Shape changes are evident along the edges of the negative crystal after 1 h as shown in Figures 1b and 1c, and become more pronounced after annealing for 4 h (Fig.1d). The morphologies suggest that cavity faces lying orthogonal to the $<10\bar{1}0>$ develop steps (ledges) but remain largely planar while faces orthogonal to $<1\bar{2}10>$ develop pairs of facets inclined to the original cavity edge.

This distinction between the behavior of $\{1\bar{2}10\}$ and $\{10\bar{1}0\}$ faces becomes more evident as the anneal time is increased. Figures 2(a-c) show the morphologies that develop after anneals of 16, 64 and 128 h, respectively. Isolated inclined steps develop on the faces lying perpendicular to the $<10\bar{1}0>$ direction. If these faces are of the $\{10\bar{1}0\}$ type, these appear to be stable, *i.e.*, components of the Wulff shape. These edges regress towards the cavity center during annealing, but remain planar. In contrast, a sawtooth profile develops on the faces perpendicular to $<1\bar{2}10>$. These observations suggest that the $\{1\bar{2}10\}$ faces are unstable, *i.e.*, not a component of the Wulff shape, and thereby unstable to breakdown into a "hill-and-valley" structure, as originally described by Herring [21]. These observations have a parallel in undoped sapphire, where experimental evidence shows that $\{1\bar{2}10\}$-type surfaces are stable and develop ledges that increase in height with anneal time, but the orthogonal $\{10\bar{1}0\}$ surfaces break down into a series of inclined facets *via* a nucleation and growth process [19, 22-24].

The instability of $\{1\bar{2}10\}$-type surfaces in silicon carbide is emphasized in the morphological evolution of features that are bounded primarily by such faces, as illustrated in Figure 3. The mask and etching conditions used also generate "channel-like" features, 1000 μm long, 10, 20, or 40 μm wide, and 0.25 μm deep. Figure 3 shows a set of such features, etched into a silicon-terminated face with the 1000 μm edge oriented perpendicular to $<1\bar{2}10>$, after 128 h at 1900°C. Geometrically similar features, when

introduced into the basal plane of sapphire develop periodic undulations that appear to be sinusoidal at similar magnifications, and channels break up by Rayleigh instabilities [6-9]. In the present case, the evolution is dominated by edge facetting. Channel pinchoff is infrequent and not periodic. In the few places where it occurs, it appears to be the result of impingement of opposing facets as they regress towards the channel center, not from the progressive amplitude increase of sinusoidal perturbations.

Circular features also develop facetted cross sections upon annealing. Figures 4a and 4b show penny-shaped flaws, 150 μm in diameter and 0.25 μm deep before and after a 128 h anneal. The (0001) projection of the cross-section is bounded by facets normal to the $<10\bar{1}0>$ directions, and is approaching a hexagonal shape. Facets of the same orientation develop regardless of whether the initial cavity perimeter is rectangular or circular. Samples were cut to expose a plane perpendicular to (0001) in an effort to determine the angle between the (0001) surface and the edge facets. Observations using scanning electron microscopy were unfortunately not able to determine the angle, and thus, it is only possible to state that facets of type $\{10\bar{1}x\}$ are stable. Further experiments are needed to completely index these facets.

Features etched into the carbon-terminated surface were also examined. Figure 5 illustrates the evolution of a rectangular cavity (200 μm × 60 μm × 0.15 μm) at 1900°C. Facetting of the $\{1\bar{2}10\}$ face is evident. In addition, traces of what appear to be ledges appear on the basal surface. These traces are oriented parallel to the $<1\bar{2}10>$ direction, and are thus consistent with the formation of $\{10\bar{1}x\}$ facets to accommodate the miscut of the crystal. The results indicate that the {0001} planes are stable.

Although there are many calculations of surface energies for low-index planes in simple ionic materials and in more complex oxides such sapphire, few surface energy calculations have been made for covalently bonded ceramics like silicon carbide. Inomata and Matsumoto [25] estimated surface energies of (pure) α-SiC $\{1\bar{2}10\}$ and $\{10\bar{1}0\}$ to be 3.88 and 3.36 J/m^2, respectively, using the sublimation energy and the density of dangling bonds on the surfaces. Decomposition of $\{1\bar{2}10\}$ facets into pairs of $\{10\bar{1}0\}$ facets would thus decrease the surface energy per unit surface area by a factor of 0.866, but this would be offset by an increase in the surface area by a factor $2/\sqrt{3}$ ($\approx$1/0.866). Decomposition into $\{10\bar{1}x\}$ facets ($x \neq 0$) would increase the total surface area by a larger factor, and would thus require a greater surface energy

reduction. Identification of the stable facets would be helpful in establishing limits on relative surface energies.

Kinetics of Pore Shape Evolution

Numerous studies have shown that undoped β-silicon carbide coarsens but does not densify readily at elevated temperature. Prochazka [26] attributed this to a high grain boundary to surface energy ratio. Prochazka proposed that when the dihedral angle is less than 60°, or equivalently, when the grain boundary to surface energy ratio, $\gamma_{gb} / \gamma_{sv}$, exceeds $\sqrt{3}$, an energetic barrier to densification exists. The observation that combined additions of boron and carbon promoted densification [26, 27] was interpreted in terms of an influence on the process energetics. Boron was assumed to segregate selectively and to selectively decrease the grain boundary energy, while carbon additions were thought to reduce the surface oxide, and remove free silicon.

Greskovich and Rosolowski [28] and Suzuki and coworkers [29-31] determined that dihedral angles in undoped β-silicon carbide were typically higher than 60°, that $\gamma_{gb} / \gamma_{sv}$ was $< \sqrt{3}$, and thus, that no energetic barrier to densification existed. This finding shifted the focus to an assessment of kinetics, specifically an assessment of the relative rates of transport *via* mechanisms that promote densification (lattice and grain boundary diffusion) versus those that promote coarsening (vapor transport and surface diffusion). The lack of densification during sintering of β-silicon carbide implied that either surface diffusion or vapor transport dominated mass transport. At sufficiently fine particle sizes, scaling law arguments [32] indicate that surface diffusion should dominate. Greskovich and Rosolowski [28] cite a negligible weight loss and the observed time dependence of the surface area reduction of β-silicon carbide during sintering as evidence that surface diffusion is the main contributor to coarsening. Suzuki and coworkers have reached similar conclusions [29-31].

Despite the potential importance of surface diffusion to processing, we are aware of no reported estimates of the surface diffusivity in α- or β-silicon carbide. As a result, efforts to examine the kinetics of pore shape evolution were undertaken, paralleling prior work on sapphire [19]. Nonequilibrium-shape pores of sizes similar to those arising during processing can be generated using lithography; the observed

pore shape evolution kinetics can then be compared to those predicted when evolution is rate-limited by surface diffusion.

Large arrays of small coin-shaped cavities (5 μm in diameter and 0.25 μm in depth) were developed using the processing methods described previously. The initial pore shape is illustrated schematically in Figure 6a; geometric and energetic parameters relevant to the kinetic modelling are also indicated. In view of the high diameter-to-depth ratio, it is unlikely that this initial shape coincides with the equilibrium shape, and shape relaxation is thus expected. The mean chemical potentials on the large circular face (FACE 1) and the thin edge face (FACE 2), $\overline{\mu}_1$ and $\overline{\mu}_2$, respectively, can be related to their weighted mean curvature (*wmc*) [33]. The weighted mean curvature of FACE 1, wmc_1, is $\left(-2\gamma_2 / r\right)$ where γ_2 is the surface energy of FACE 2, and r is the radius of FACE 1, as shown in Figure 6a. For FACE 2, wmc_2 is $-\left((\gamma_1 / l)+(\gamma_2 / r)\right)$ where γ_1 is the surface energy of FACE 1, and $2l$ is the depth of FACE 2. The driving force for transfer of atoms from FACE 1 to FACE 2 can then be expressed as

$$\begin{aligned}\Delta\overline{\mu}_{1\to 2} &= \overline{\mu}_2 - \overline{\mu}_1 = \left(\mu_o + \overline{V}(wmc)_2\right) - \left(\mu_o + \overline{V}(wmc)_1\right) \\ &= \overline{V}\left[\frac{\gamma_2}{r} - \frac{\gamma_1}{l}\right]\end{aligned} \tag{1}$$

where $\overline{V}$ is the molar volume. If $\gamma_1 = \gamma_2 = \gamma$, then $\Delta\mu_{1\to 2}$ will be negative when $l < r$, as in the present initial shape. The resulting hypothetical equilibrium shape (assuming that no new facets form) is represented by Figure 6b.

Representative optical micrographs illustrating the time evolution of the pore shape within a specific 48-pore array are shown in Figure 7. Figure 7a illustrates the pore morphology after bonding but prior to any high temperature annealing. The same subarray, after anneals of 4 h (14.4 ks), 16 h (57.6 ks), and 128 h (460.8 ks) at 1900°C is shown in Figures 7b, 7c, and 7d, respectively. It is evident that some lateral contraction does occur; there is also evidence of edge facetting, indicating that new facets do develop, paralleling the behavior in Figure 4. It is interesting to note that the facetting is not as pronounced as in Figure 4. Further discussion of this issue is deferred to a later section of the paper.

To quantify the shape change rate, the projected surface area of the cavities was measured after each anneal period. Figure 8 plots the time dependence of the ratio $A_t / A_{t=0}$, where A_t is the projected cross-sectional area of the cavity after annealing for time *t*, and $A_{t=0}$ is the original projected cross-sectional area. The reported value of A_t is the average of the projected surface area of the cavities in several optical micrographs, each of which record the evolution of distinct 48 cavity arrays, similar to Figures 7a-d. In view of the observations that silicon carbide is difficult to densify, and that in the present case contributions to densification from grain boundary diffusion are minimized,❖ it was assumed that the cavity volume remains constant.

The measured pore shape evolution rates can be compared with the predicted rates for the shape relaxation of a coin-shaped cavity. Prior work by Yu and Hackney [34], and by Carter *et al.* [35] has treated the problem of surface diffusion rate limited evolution of a fully facetted 2-D cavity or particle of constant volume. The surface flux, J_s, can be related to the gradient in the chemical potential at the surface. Fick's first law of diffusion for the surface flux (in atoms/m^2•s) can be written as

$$J_s = -\frac{D_s}{\overline{V}\mathrm{k}T} \bullet \frac{d\mu}{dx} \tag{2}$$

where D_s is the surface diffusion coefficient, $\overline{V}$ is the molar volume, k is Boltzmann's constant, and T is absolute temperature. The local rate of mass accumulation, and thus the surface displacement rate, hinges on the gradient in the flux. The normal velocity of a surface, V_n can be expressed as

$$V_n = -\frac{dJ_s}{dx}\delta_s\Omega = \frac{\delta_s D_s}{\mathrm{k}T} \bullet \left(\frac{d^2\mu}{dx^2}\right) \tag{3}$$

where δ_s is the width over which diffusion is enhanced, and Ω is the atomic volume. In order to displace facets uniformly, the surface potential must vary continuously with position on the facet such that $\nabla^2\mu$ is constant on each facet. A parabolic variation of the potential with position results.

❖ During bonding of the etched and unetched single crystal, efforts are made to perfectly align the two crystals such that a 0° twist boundary is introduced. In practice, small misalignments, of the order of 1-2° can arise, resulting in a low-angle grain boundary. In the present case, two distinct crystals, a Si-terminated and a C-terminated crystal, each with a distinct miscut are bonded to internalize the pore arrays. As a result, differences in the miscut of the two crystals may also contribute to the misorientation between the two single crystals. However, we do not expect this misorientation to exceed a few degrees, and thus, even in the worst case, the contribution of grain boundary diffusion to pore shrinkage should be negligible.

The extension of such parabolic potential (*pp*) models to 3-D shapes of the type examined in this and prior studies on sapphire [19] is generally difficult. Kitayama *et al.* [19, 36] have shown that in both 2-D and 3-D cases, evolution rates can be estimated by focussing on the gradient at the facet edge, and approximating the potential gradient at the edge as the difference in the mean potentials, Eqn. (1), scaled by an appropriate distance. For the coin-shaped cavities, the potential will be either a minimum or maximum at the facet centers, and either a maximum or minimum at the facet edges, depending upon whether the facet acts a mass sink (FACE 2) or a mass source (FACE 1). If the center-to-edge variation of potential with position is linearized, and Eqn. (1) defines the mean potentials, then the potential is at its mean value for FACE 1 and FACE 2 at distances of ≈½*r* and ½*l* from the shared edge. The sum of these distances is used to scale the potential difference, and estimate the potential gradient, and thus the mass arrival/removal rate from the facets. The details of this method, and a derivation of the evolution rate are provided in Reference [19].

For simplicity, the energies of the two faces, γ_1 and γ_2, are assumed equal. It is reasonable to assume that the cavity volume V_C is constant. If the cross-section is taken to be circular, then the radius at time *t* can be calculated from A_t. The equilibrium value of *r* becomes $\left(V_C / 2\pi\right)^{1/3}$. With the stated assumptions, and using the variable definitions in Figure 6, the methods detailed in Reference [19] yield an expression for the time dependence of the cavity radius

$$\left(\frac{dr}{dt}\right)_{lp} = \frac{D_s \Omega^{4/3} \gamma}{kT} \cdot \frac{8\pi^2 r^3}{V_C^2} \cdot \frac{\left(V_C - 2\pi r^3\right)}{\left(V_C + 2\pi r^3\right)} \tag{4}$$

where Ω is the atomic volume. For this simple geometry, it is also possible to derive an equation for the spatial variation of the chemical potential, and to predict the time dependence of *r* for the parabolic potential

$$\left(\frac{dr}{dt}\right)_{pp} = \frac{D_s \Omega^{4/3} \gamma}{kT} \cdot \frac{12\pi^2 r^3}{V_C^2} \cdot \frac{\left(V_C - 2\pi r^3\right)}{\left(V_C + 1.5\pi r^3\right)} \tag{5}$$

Both Eqns. (4) and (5) can be integrated, and the time dependence of $A_t / A_{t=0}$ can be predicted.

Figure 9 compares the experimental results (*filled circles*) with the predictions based on Eqns. (4) and (5).[✠] The calculations assume a temperature of 1900°C. The Si-C pair volume in 6H α-SiC (2.07×10^{-29} m^3) was used for Ω. A value of 1 J/m^2 was used for γ. We note that calculations by Pearson *et al.* [37] predict the surface energy of 3C β-silicon carbide (111) silicon- and $(\bar{1}\bar{1}\bar{1})$ carbon-faces to be 2.2 and 0.3 J/m^2, respectively. The atomic configurations of 6H α-silicon carbide (0001) silicon- and $(000\bar{1})$ carbon faces are identical to those of the 3C β-silicon carbide (111) silicon- and $(\bar{1}\bar{1}\bar{1})$ carbon-faces, respectively. The cavity volume was taken to be 4.91×10^{-18} m^3, and assumed constant. Since there have been no prior reports of the surface diffusivity in silicon carbide at high temperature, values of 10^{-12} and 10^{-14} m^2/s were used for calculations. The observed shape evolution trajectory bridges the predicted trajectories for these two values of D_s. After 4 h (14.4 ks), the experimental $A_t / A_{t=0}$ falls on the predicted trajectory for $D_s = 10^{-12}$ m^2/s, however, as the anneal time increases, the evolution rate decays more rapidly than predicted for surface-diffusion-controlled evolution. At 128 h (460.8 ks), the behavior is more nearly consistent with $D_s = 10^{-14}$ m^2/s. Thus, the *apparent* surface diffusivity is decreasing with time.

Parallel observations have been made in studies of pore shape relaxation in sapphire. When cavities of nonequilibrium shape were etched into stable surfaces, especially the (0001) surface of sapphire, the evolution rate also decreased more rapidly than expected for surface-diffusion-controlled evolution. This rapid decrease in evolution rate was interpreted as suggesting that in cases where cavities (or particles) are bounded by stable facets, the evolution rate becomes limited by the availability of attachment or detachment sites. In general, the miscut of the crystals is small, and for small cavities, surface irregularities (ledges) due to miscut, scratches, and nonuniform ion beam etching will be removed as the shape changes. Once flat and stable facets are formed, adjusting the aspect ratio of the pore requires the nucleation of patches of adatoms on surfaces that must advance towards the pore center, and the nucleation of critical size cavities in surfaces that must recede from the pore center as the equilibrium shape is approached. These nucleation processes are likely to occur at a low and declining rate as the driving force for

[✠] Although the calculations assume that $\gamma_1 = \gamma_2 = \gamma$, prior modelling work describing the evolution of 2-D features indicates that small variations in the γ_1 / γ_2 ratio does substantially alter the evolution kinetics. We expect the same to be true in the 3-D case treated here.

morphological change decreases. If screw dislocations are not present to provide a sufficiently large and time-independent source of ledges for attachment or detachment of adatoms, then the evolution rate will decay, and ultimately be limited by the rate at which ledges can be supplied by nucleation processes on facets that act as mass sources and sinks. Recent calculations by Mullins and Rohrer [38] suggest that the barrier to the nucleation of new facet layers is extremely large for facets above a limiting size of ≈1 nm, making particles/cavities without alternative sources of ledges (dislocations) unable to adjust their shape. In contrast, if cavities are etched into unstable surfaces, *e.g.*, the $\mathbf{m}\{10\bar{1}0\}$ plane in sapphire, decomposition of these surfaces into hill-and-valley structures is observed [23]; cavities bounded primarily by such unstable planes undergo rapid morphological change at rates approximately consistent with a surface diffusion analysis [19].

The facetting study, and in particular Figure 5, indicates that the {0001} surfaces of 6H α-silicon carbide are stable. Thus, arguments similar to those applied to sapphire may be appropriate, and explain the rapid decay of the evolution rate. The possible role of dislocations as ledge sources can also be assessed. The dislocation density in 6H α-silicon carbide wafers (from the same source employed here) has been measured by several investigators, and ranges from 10^3 to $10^4/\text{cm}^2$ [39]. Using $10^4/\text{cm}^2$, this translates to an area of 10^4 μm^2 per dislocation. If dislocations are randomly distributed, the probability that a 5 μm diameter area will intersect a dislocation is roughly 1 in 510. The probability that *both* opposing 5 μm diameter faces of a pore intersect a dislocation is 1 in $\approx 2.6 \times 10^5$. Statistically it thus seems unlikely that dislocations would provide a viable ledge source for these smaller pores. Although the degree of evolution varied within arrays of these fine pores, none evolved to the degree that the larger pores, such as those shown in Figure 4 evolved. For these 150 μm-diameter cavities, the area per circular face is $\approx 1.8 \times 10^4$ μm^2. As a result, on average *both* faces will intersect *at least* one dislocation. We note that most pores of this size developed well-formed facets, and only a small fraction did not evolve to an extent similar to that illustrated in Figure 4b. These observations strongly support the notion that evolution of the finer cavities is limited by availability of ledges. Experiments using crystals with larger miscut or mechanically treated to increase the dislocation density would be helpful in testing this hypothesis. To our knowledge, α-silicon carbide single crystals with surface orientations that appear to be unstable, *e.g.*, the $\{1\bar{2}10\}$ face, are unfortunately

not commercially available. Measurements of shape evolution rates of pores etched into such surfaces may provide an estimate of D_s that would be more applicable to sintering.

Summary and Conclusions

The results demonstrate that it is possible to apply microlithography and bonding methods to introduce controlled-geometry internal defects in 6H silicon carbide single crystals. These internal cavities provide the basis for studies of facetting and morphological evolution using methods similar to those applied previously to sapphire.

Facetting along the perimeter of cavities of varying shapes and size was observed after anneals of 1 h at 1900°C. Decomposition of $\{1\bar{2}10\}$ faces into $\{10\bar{1}x\}$faces was evident after 16 h anneals, demonstrating that $\{1\bar{2}10\}$ faces are not components of the Wulff shape at 1900°C. Further studies will be necessary to fully characterize the equilibrium facets.

The experimentally observed evolution rates of coin-shaped cavities towards an equilibrium shape decreased more rapidly than those expected when surface diffusion controls the evolution rate. If surface diffusion controls the evolution rate, it does so only during the very initial stages. In view of the tendency to form facets, the results suggest that during the later stages, morphological evolution in this system is limited by the nucleation rate of attachment/detachment sites (ledges) on the facets. Similar interpretations have been applied to an analysis of pore shape changes in sapphire.

Acknowledgements

This research was supported by the Director, the Office of Energy Research, Office of Basic Energy Sciences, Materials Sciences Division of the U.S. Department of Energy under Contract No. DE-AC03-76SF00098. One of the authors (TN) was supported by the Ministry of Education, Science, Sports and Culture, Japan under contract No.9-Young Scientists-15. The authors would like to express their gratitude to the staff of the Microfabrication Laboratory at the University of California at Berkeley for helping to make the experimental component of this research possible. We also thank Professor Ronald Gronsky, Mr. Robert Marks (University of California, Berkeley) and Professor Mikito Kitayama (Fukuoka Institute of Technology, Fukuoka, Japan) for useful suggestions and discussion. We particularly wish to express our gratitude to the reviewers and associate editor for their numerous useful comments and suggestions. The paper has benefitted significantly from their input.

References

[1] T. K. Gupta, "Instability of Cylindrical Voids in Alumina," *J. Am. Ceram. Soc.*, **61**, [5-6], 191-95 (1978).

[2] T. K. Gupta, "Crack Healing in Al_2O_3, MgO, and Related Materials," pp. 750-66 in Advances in Ceramics, Vol. 10, W. D. Kingery, Ed. Columbus: The American Ceramic Society, 1984.

[3] J. Rödel and A. M. Glaeser, "Production of controlled-morphology pore arrays: implications and opportunities," *J. Am. Ceram. Soc.*, **70**, [8], C172-5 (1987).

[4] J. Rödel and A. M. Glaeser, "Microdesigned Interfaces: New Opportunities for Materials Science," *J. Ceram. Soc. Japan*, **99**, [4], 251-65 (1991).

[5] J. Rödel and A. M. Glaeser, "High-Temperature Healing of Lithographically Introduced Cracks in Sapphire," *J. Am. Ceram. Soc.*, **73**, [3], 592-601 (1990).

[6] J. D. Powers and A. M. Glaeser, "High-Temperature Healing of Cracklike Flaws in Mg- and Ca-Ion-Implanted Sapphire," *J. Am. Ceram. Soc.*, **75**, [9], 2547-58 (1992).

[7] J. D. Powers and A. M. Glaeser, "High-Temperature Healing of Cracklike Flaws in Titanium Ion-Implanted Sapphire," *J. Am. Ceram. Soc.*, **76**, [9], 2225-34 (1993).

[8] J. Rödel and A. M. Glaeser, "Morphological Evolution of Pore Channels in Alumina," pp. 243-57 in Sintering of Advanced Ceramics, Vol. 7, *Ceramic Transactions*, C. A. Handwerker, J. E. Blendell, and W. A. Kaysser, Eds. Westerville, OH: The American Ceramic Society, 1990.

[9] L. Kulinsky, J. D. Powers, and A. M. Glaeser, "Morphological Evolution of Pre-perturbed Pore Channels in Sapphire," *Acta Mater.*, **44**, [10], 4115-30 (1996).

[10] M. Kitayama, "The Wulff Shape of Doped and Undoped Sapphire," Ph.D. thesis, Department of Materials Science and Mineral Engineering, University of California, Berkeley, (1996).

[11] M. Kitayama, J. D. Powers, L. Kulinsky, and A. M. Glaeser, "Surface and interface properties of alumina via model studies of microdesigned interfaces," *J. Eur. Ceram. Soc.*, **19**, [13-14], 2191-209 (1999).

[12] M. Srinivasan, "The Silicon Carbide Family of Structural Ceramics," pp. 99-160 in Structural Ceramics, Vol. 29, *Treatise on Materials Science and Technology*, J. B. Wachtman, Ed. London: Academic Press, 1989.

[13] W. von Munch and P. Hoeck, "Silicon carbide bipolar transistor," *Solid-State Electron.*, **21**, [2], 479-80 (1978).

[14] S. Nishino, A. Ibaraki, H. Matsunami, and T. Tanaka, "Blue-emitting diodes of 6H-SiC prepared by chemical vapor deposition," *Jap. J. Appl. Phys.*, **19**, [7], L353-6 (1980).

[15] S. Yoshida, K. Sasaki, E. Sakuma, S. Misawa, and S. Gonda, "Schottky barrier diodes on 3C-SiC," *Appl. Phys. Lett.*, **46**, [8], 766-8 (1985).

[16] M. Shinohara, M. Yamanaka, S. Misawa, H. Okumura, and S. Yoshida, "C-V characteristics of MOS structures fabricated of Al-doped p-type 3C-SiC epilayers grown on Si by chemical vapor deposition," *Jap. J. Appl. Phys., Pt. I*, **30**, [2], 240-3 (1991).

[17] R. A. Stein, P. Lanig, and S. Leibenzeder, "Influence of Surface Energy On the Growth of 6H-SiC and 4H-SiC Polytypes By Sublimation," *Mater. Sci. Eng. B*, **11**, [1-4], 69-71 (1992).

[18] T. Kimoto and H. Matsunami, "Surface Diffusion Lengths of Adatoms On 6H-SiC(0001) Faces in Chemical Vapor Deposition of SiC," *J. Appl. Phys.*, **78**, [5], 3132-3137 (1995).

[19] M. Kitayama, T. Narushima, and A. M. Glaeser, "The Wulff Shape of Alumina: II. Experimental Measurement of Pore Shape Evolution," *J. Am. Ceram. Soc.*, **83**, [10], 2572-2583 (2000).

[20] J. Pezoldt, B. Stottko, G. Kupris, and G. Ecke, "Sputtering effects in hexagonal silicon carbide," *Mater. Sci. Eng., B*, **B29**, [1-3], 94-8 (1995).

[21] C. Herring, "Some Theorems on the Free Energy of Crystal Surfaces," *Phys. Rev.*, **82**, [1], 87-93 (1951).

[22] J. R. Heffelfinger, M. W. Bench, and C. B. Carter, "On the faceting of ceramic surfaces," *Surf. Sci.*, **343**, [1-2], L1161-6 (1995).

[23] J. R. Heffelfinger and C. B. Carter, "Mechanisms of surface faceting and coarsening," *Surf. Sci.*, **389**, [1-3], 188-200 (1997).

[24] J. R. Heffelfinger, M. W. Bench, and C. B. Carter, "Steps and the structure of the (0001) α-alumina surface," *Surf. Sci.*, **370**, [1], L168-72 (1997).

[25] Y. Inomata and S. Matsumoto, "On the formation of β-SiC in the initial growth stage," *Yogyo-Kyokai-Shi*, **79**, [1], 30-36 (1971).

[26] S. Prochazka, "The Role of Boron and Carbon in the Sintering of Silicon Carbide," pp. 171-181 in Special Ceramics 6, P. Popper, Ed. Manchester: The British Ceramic Research Association, 1975.

[27] S. Prochazka and R. M. Scanlan, "Effect of boron and carbon on sintering of SiC," *J. Am. Ceram. Soc.*, **58**, [1], 72 (1975).

[28] C. Greskovich and J. H. Rosolowski, "Sintering of covalent solids," *J. Am. Ceram. Soc.*, **59**, [7-8], 336-43 (1976).

[29] H. Suzuki and T. Hase, "Some Experimental Consideration on the Mechanism of Pressureless Sintering of Silicon Carbide," pp. 345-365 in Proceedings of International Symposium of Factors of Densification and Sintering of Oxide and Non-Oxide Ceramics. Hakone, Japan, October 3-5, 1978.

[30] T. Hase, H. Suzuki, and I. Tomizuka, "Microstructure Development of Undoped Compact of β-SiC during Heating," *Yogyo-Kyokai-Shi*, **87**, [6], 47-51 (1979).

[31] H. Suzuki, "Recent Trends and Theoretical Background in Sintering of Silicon Carbide Ceramics," *Seramikkusu*, **18**, [1], 3-9 (1983).

[32] C. Herring, "Effect of Change of Scale on Sintering Phenomena," *J. Appl. Phys.*, **21**, [4], 301-03 (1950).

[33] J. E. Taylor, "Overview No. 98 II – Mean Curvature and Weighted Mean Curvature," *Acta Metall. Mater.*, **40**, [7], 1475-85 (1992).

[34] S. H. Yu and S. A. Hackney, "On the shape change of a nonequilibrium faceted microcrystal," *Scripta Metall. Mater.*, **24**, [11], 2077-82 (1990).

[35] W. C. Carter, A. R. Roosen, J. W. Cahn, and J. E. Taylor, "Shape Evolution by Surface Diffusion and Surface Attachment Limited Kinetics on Completely Facetted Surfaces," *Acta Metall. Mater.*, **43**, [12], 4309-4323 (1995).

[36] M. Kitayama, T. Narushima, W. C. Carter, R. M. Cannon, and A. M. Glaeser, "The Wulff Shape of Alumina: I. Modelling the Kinetics of Morphological Evolution," *J. Am. Ceram. Soc.*, **83**, [10], 2561-2571 (2000).

[37] E. Pearson, T. Takai, T. Halicioglu, and W. A. Tiller, "Computer modeling of Si and SiC surfaces and surface processes relevant to crystal growth from the vapor," *J. Cryst. Growth*, **70**, [1], 33-40 (1984).

[38] W. W. Mullins and G. S. Rohrer, "Nucleation barrier for volume-conserving shape changes of faceted crystals," *J. Am. Ceram. Soc.*, **83**, [1], 214-16 (2000).

[39] M. Dudley, S. P. Wang, W. Huang, C. H. Carter, V. F. Tsvetkov, and C. Fazi, "White-Beam Synchrotron Topographic Studies of Defects in 6H-SiC Single Crystals," *J. Phys. D-Appl. Phys.*, **28**, [SI], A63-A68 (1995).

Figure Captions:

Figure 1 Optical micrographs of a "rectangular" cavity (a) before, and (b-d) after progressively longer anneals at 1900°C. Figures (b) and (c) show the cavity at lower and higher magnification after a 1 h anneal. Figure (d) shows the defect after a total anneal time of 4 h.

Figure 2 Optical micrographs illustrating the morphology of an initially "rectangular" cavity after total anneal times of (a) 16 h, (b) 64 h, and (c) 128 h at 1900°C.

Figure 3 Optical micrograph of sections of 1000 μm long, 0.25 μm deep pore channels of varying initial width after 128 h at 1900°C. The pore channel axes are aligned parallel to a $<10\bar{1}0>$ direction.

Figure 4 Optical micrographs of an initially "circular" coin-shaped cracklike cavity (a) before and (b) after 128 h at 1900°C.

Figure 5 Optical micrographs illustrating the morphology of an initially "rectangular" cavity after 128 h at 1900°C. The ledges and facets evident on the (0001) face presumably accommodate the miscut of the crystal surface.

Figure 6 Geometry of the coin-shaped cavities. In a) the geometric and energetic parameters of the initial shape are illustrated. For the simplified case considered, b) illustrates the hypothetical equilibrium shape. (It is presumed that face 1 remains a facet during evolution, and that $\gamma_1 = \gamma_2$.) Prior work indicates that different assumptions regarding the initial geometry [19, 36] and the relative surface energies [36] have only a minor effect on the predicted evolution kinetics.

Figure 7 Optical micrographs illustrating the morphology of the same 48 cavity array a) after bonding, but prior to any annealing, and after anneals of (b) 4 h, (c) 16 h, and (d) 128 h at 1900°C. (Bar = 20 μm)

Figure 8 Time dependence of the ratio of the projected area of the circular defects after anneal time t (A_t) to their original projected area ($A_{t=0}$). Points represent the mean value; the error bars represent the standard deviation of the area ratios for the arrays evaluated.

Figure 9 Comparison of the observed time evolution of the ratio $A_t / A_{t=0}$ (filled circles) versus that predicted for surface-diffusion-controlled evolution. Two values for the surface diffusivity and two modelling approaches are considered.

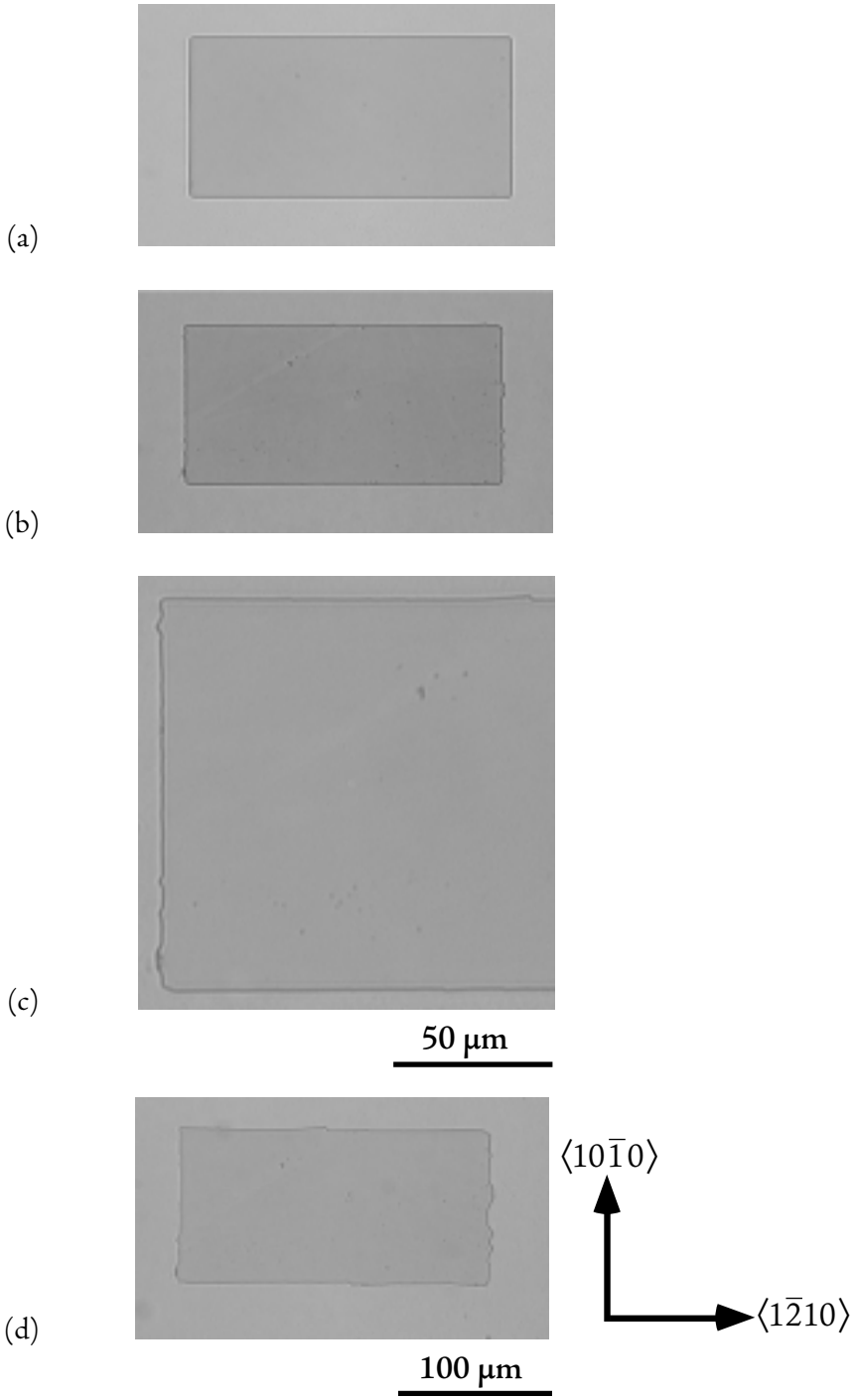

Figure 1 Optical micrographs of a "rectangular" cavity (a) before, and (b-d) after progressively longer anneals at 1900°C. Figures (b) and (c) show the crack at lower and higher magnification after a 1 h anneal. Figure (d) shows the crack after a total anneal time of 4 h.

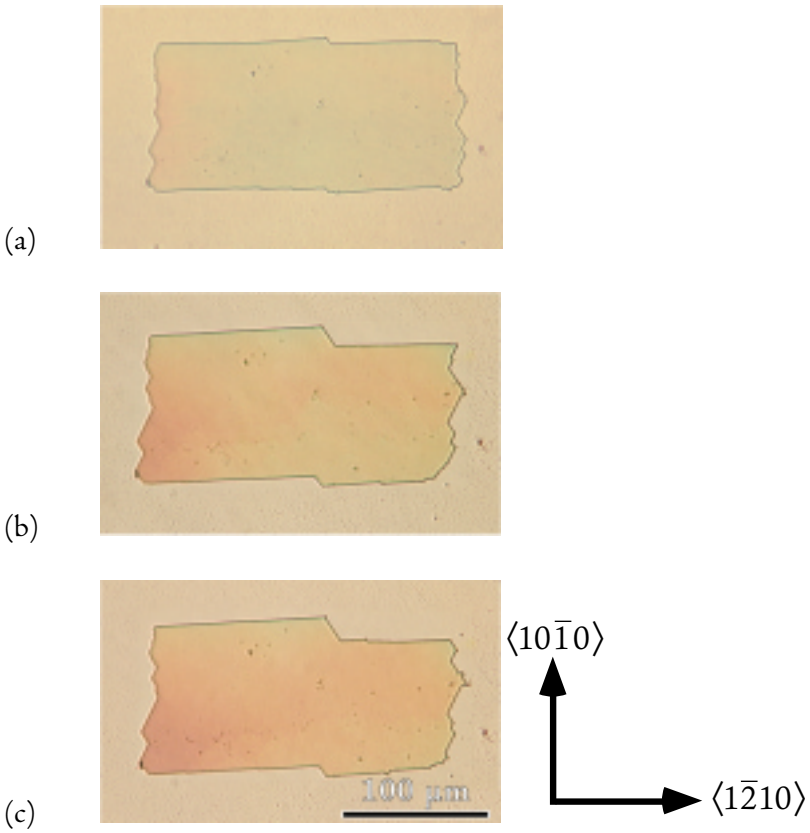

Figure 2 Optical micrographs illustrating the morphology of an initially "rectangular" cavity after total anneal times of (a) 16 h, (b) 64 h, and (c) 128 h at 1900°C.

Figure 3 Optical micrograph of sections of 1000 μm long, 0.25 μm deep pore channels of varying initial width after 128 h at 1900°C. The pore channel axes are aligned parallel to a <10$\bar{1}$0> direction.

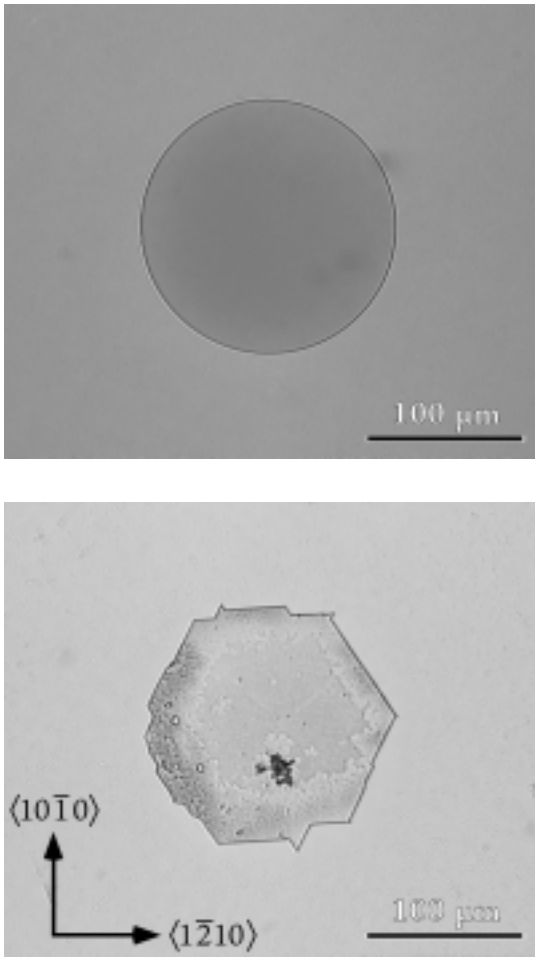

(a)

(b)

Figure 4 Optical micrographs of an initially "circular" coin-shaped cracklike cavity (a) before and (b) after 128 h at 1900°C.

Figure 5 Optical micrographs illustrating the morphology of an initially "rectangular" cavity after 128 h at 1900°C. The ledges and facets evident on the (0001) face presumably accommodate the miscut of the crystal surface.

(a) Initial state (*not to scale*)

$r = 2.5\ \mu\text{m}$

$l = 0.125\ \mu\text{m}$

$V_C = 4.91 \times 10^{-18}\ \text{m}^3$

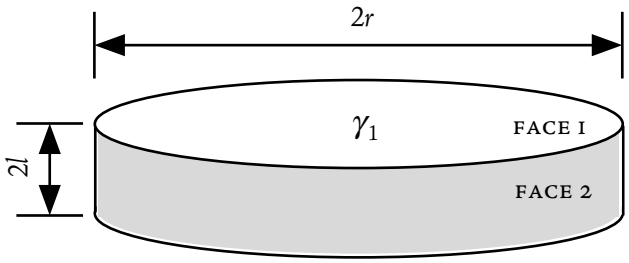

(b) Final state

$r = 0.92\ \mu\text{m}$

$l = 0.92\ \mu\text{m}$

$V_C = 4.91 \times 10^{-18}\ \text{m}^3$

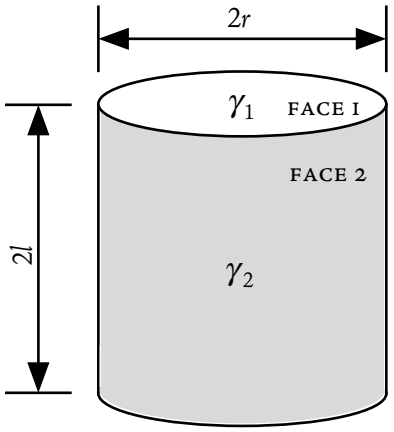

Figure 6 Geometry of the coin-shaped cavities. In a) the geometric and energetic parameters of the initial shape are illustrated. For the simplified case considered, b) illustrates the hypothetical equilibrium shape. (It is presumed that FACE 1 remains a facet during evolution, and that $\gamma_1 = \gamma_2$.) Prior work indicates that different assumptions regarding the initial geometry [19, 36] and the relative surface energies [36] have only a minor effect on the predicted evolution kinetics.

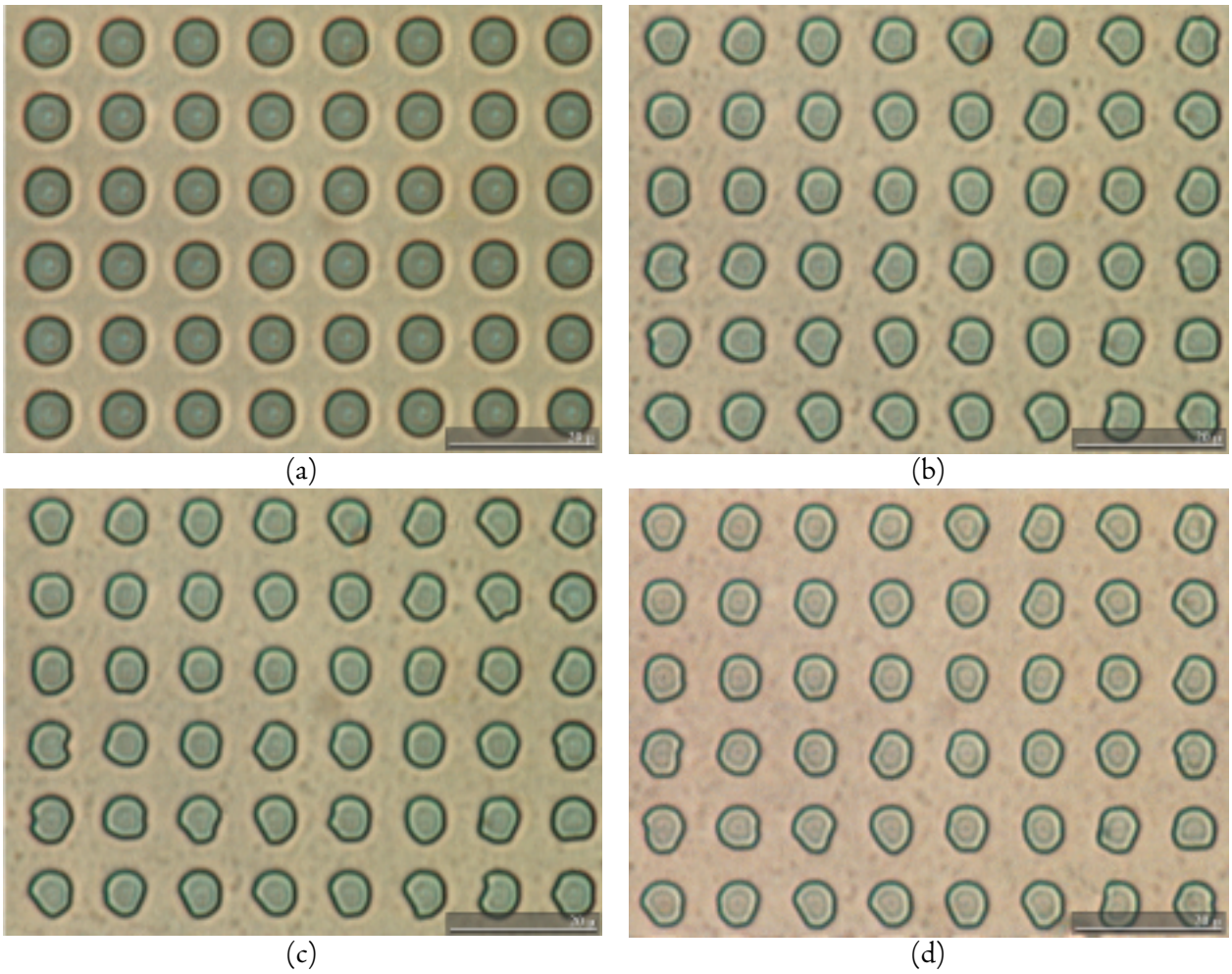

Figure 7 Optical micrographs illustrating the morphology of the same 48 cavity array a) after bonding, but prior to any annealing, and after anneals of (b) 4 h, (c) 16 h, and (d) 128 h at 1900°C. (Bar = 20 μm)

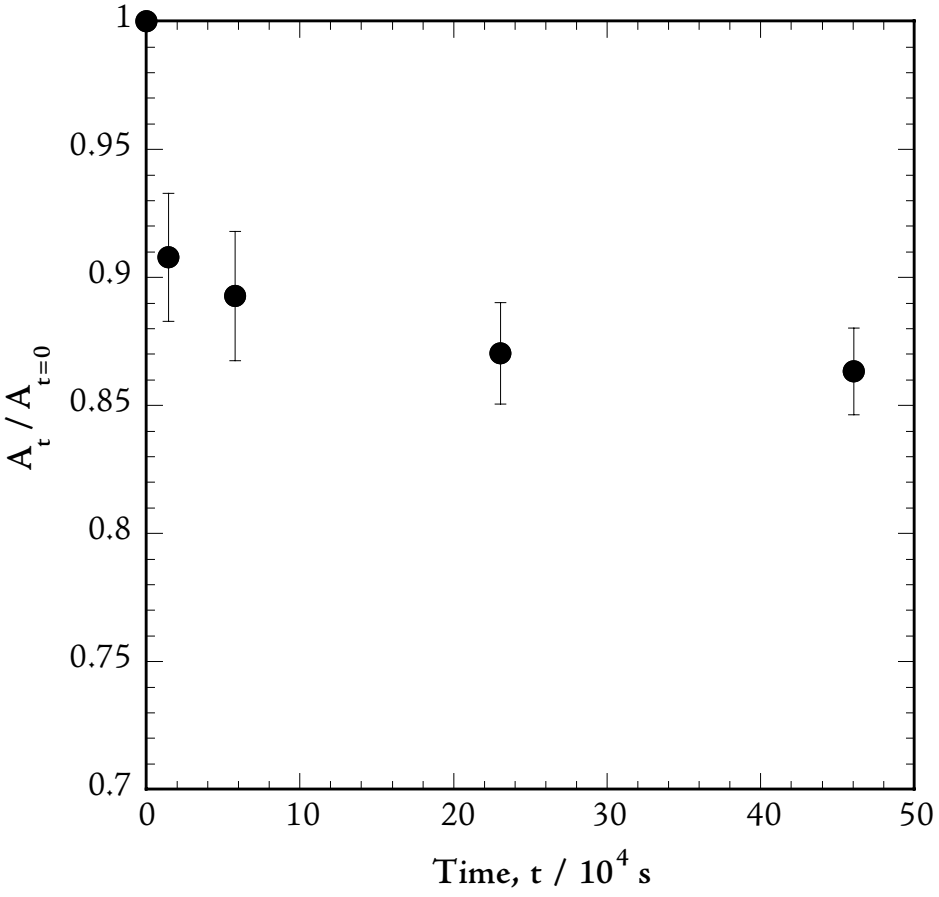

Figure 8 Time dependence of the ratio of the projected area of the circular defects after anneal time t (A_t) to their original projected area ($A_{t=0}$). Points represent the mean value; the error bars represent the standard deviation of the area ratios for the arrays evaluated.

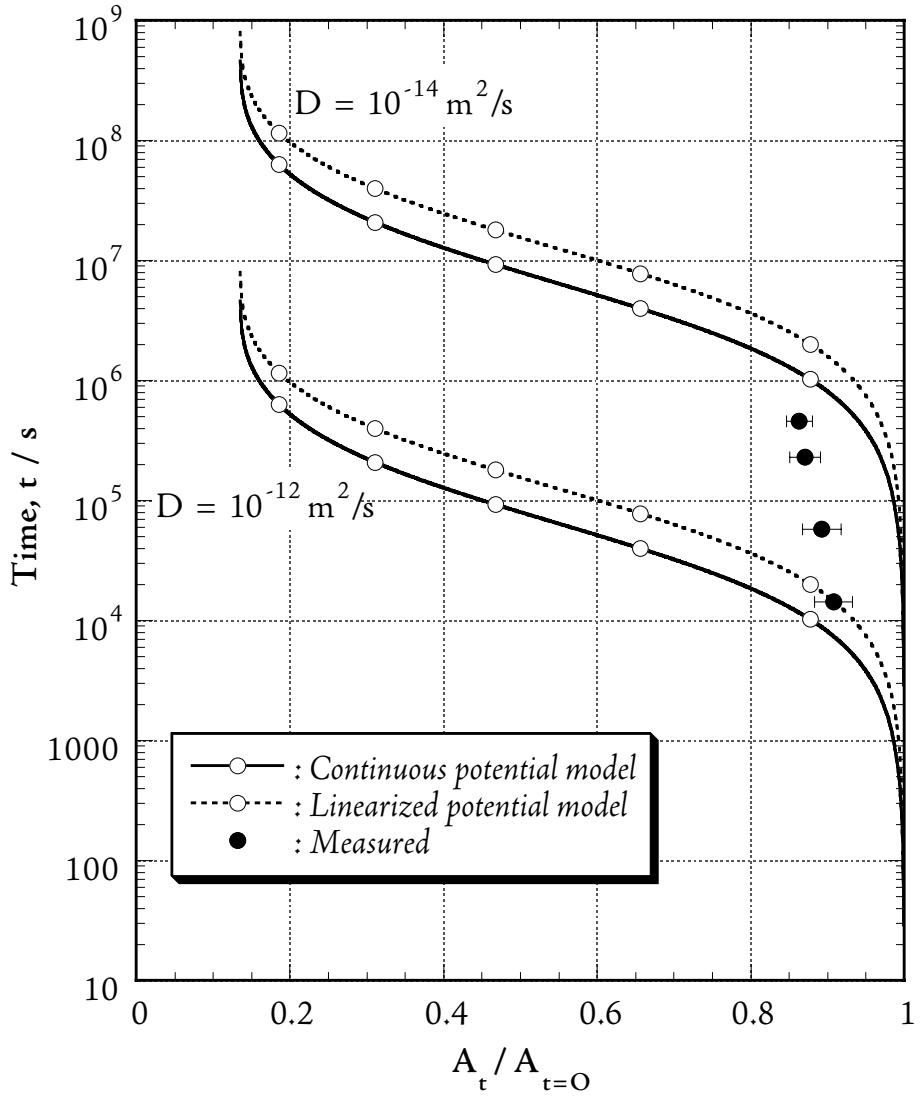

Figure 9 Comparison of the observed time evolution of the ratio $A_t / A_{t=0}$ (filled circles) versus that predicted for surface-diffusion-controlled evolution. Two values for the surface diffusivity and two modelling approaches are considered.